Optics Communications 285 (2012) 2122–2127

Contents lists available at SciVerse ScienceDirect

Optics Communications

journal homepage: www.elsevier.com/locate/optcom

Laser diode end-pumped passively Q-switched Tm,Ho:YLF laser with Cr:ZnS as a saturable absorber

Xinlu Zhang *, Xiujuan Bao, Li Li, Hong Li, Jinhui Cui

College of Science, Harbin Engineering University, Harbin 150001, China

ARTICLE INFO

Article history:
Received 8 September 2011
Received in revised form 14 November 2011
Accepted 21 December 2011
Available online 4 January 2012

Keywords:
Diode pumped lasers
Tm,Ho:YLF
Cr:ZnS
Passively Q-switched lasers

ABSTRACT

Output performance of a continuous-wave (CW) laser diode end-pumped passively Q-switched Tm,Ho:YLF laser is demonstrated with a Cr:ZnS crystal as the saturable absorber. We particularly investigate the influence of saturable absorber's position in the resonator when the Cr:ZnS crystal is placed close to and far from the laser beam waist. We compare the experimental results at the two different positions, and find that the laser shows unusual output characteristics when the Cr:ZnS saturable absorber is placed close to the beam waist. The pulse width and the pulse energy almost keep constant, measured about 1.25 μs and 4 μJ respectively, when the pump power is changed in the range of 1–1.9 W. Moreover, the pulse repetition frequency can be tuned between 1.3 kHz and 2.6 kHz by changing the pump power. The output wavelength of the passively Q-switched laser shifts to 2053 nm from 2067 nm in CW operation.

1. Introduction

Eye-safe, diode-pumped all-solid-state lasers operating in the spectral region near 2 μm are regarded as promising sources for various applications in Doppler wind sensing, differential absorption lidar, water vapor profiling, and low altitude wind shear detection [1,2]. The Tm-Ho co-doped materials, operating on the Ho transition, are usually preferred for high-output energy application, many different hosts and transitions have been reported to laser [3–7]. Continuous wave and actively Q-switched Tm,Ho:YLF lasers have been widely investigated [8–12], but few papers have reported on the microsecond pulse passively Q-switched Tm,Ho:YLF lasers at present.

Passive Q-switching is more cost-effective and simpler method to provide compact setups, furthermore it does not need rather expensive and bulky acousto-optic or electro-optic modulators. However, only few passive Q-switching experiments have been performed at 2 μm wavelength range. Y. K. Kuo et al. reported the flashlamp-pumped passively Q-switched 2 μm Tm,Cr:$Y_3Al_5O_{12}$ lasers with Ho:YVO_4, Ho:$YLiF_4$ and Ho:GaF_2 crystals as effective solid-state saturable absorbers respectively [13–15]. Flash-lamp-pumped Ho:YAG (2090 nm) and Tm:YAG (2017 nm) passively Q-switched lasers by use of a Cr:ZnSe saturable absorber also were reported [16]. Passively Q-switched Yb,Tm:$KY(WO_4)_2$ and Tm:$KY(WO_4)_2$ lasers with a thin plate of Cr:ZnS as a saturable absorber also were presented, and a maximum average output power of 116 mW emitted at 1.9 μm was obtained [17]. Yao et al. demonstrated a passively Q-switched operation of a diode pumped Tm:YAP laser by using a semiconductor saturable absorber based on InGaAs/GaAs at the wavelengths 1940 nm and 1986 nm, however, the passively Q-swithed Tm:YAP laser has a high threshold pump power of about 15 W [18]. At the same time, the passively Q-switched Tm fiber lasers also got good development. Qamar et al. presented passively Q-switched pulses with 330 ns pulse duration and 15 W peak power using a single-clad Tm-silica fiber laser and Cr:ZnSe saturable absorber crystal at 1.9 μm when pumped with 3.6 W launched power at 1.3 μm [19]. Jackson reported an all-fiber passively Q-switched double-clad Tm-doped fiber laser with Ho-doped silica fiber as a saturable absorber [20].

In this paper, we describe a stable pulse-width passively Q-switched Tm,Ho:YLF laser which generates nearly diffraction-limited laser beam at 2053 nm. The pulse width is about 1.25 μs, the pulsed energy is about 4 μJ, and the pulse repetition frequency is between 1.3 kHz and 2.6 kHz that can be tuned by changing the pump power. The nearly diffraction-limited and stable long pulse laser can be used to laser lidar systems for accurate wind velocity measurements. For coherent laser lidar, an accurate wind velocity measurement requires microsecond pulses [21]. Injection seeding by a long pulse seed laser can directly produce pulses of the proper duration without requiring excessively long resonators or elaborate cavity-loss control schemes [22].

2. Experimental setup

The experimental setup is shown in Fig. 1. The pump laser is a fiber-coupled laser diode temperature-tuned to 792 nm emission wavelength. The diameter and numerical aperture of the fiber core are 100 μm and 0.22 respectively. A coupling optics system is used

* Corresponding author at: College of Science, Harbin Engineering University, 145 Nan Tong Da Jie, Harbin, 150001, China. Tel./fax: +86 451 82519754.
E-mail address: zhangxinlu1@yahoo.com.cn (X. Zhang).

0030-4018/$ – see front matter © 2012 Elsevier B.V. All rights reserved.
doi:10.1016/j.optcom.2011.12.081

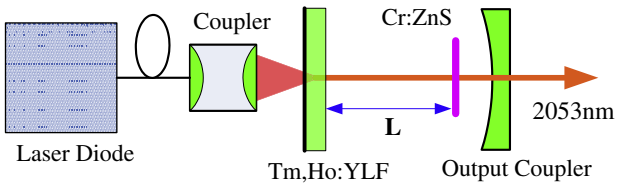

Fig. 1. Schematic diagram for the passively Q-switched Tm,Ho:YLF laser.

to focus the pump beam. The total transmission efficiency of the beam-reshaping system is over 90% at 792 nm.

The a-cut Tm,Ho:YLF laser crystal has dopant concentrations (with respect to the Y-lattice site) of 6% Tm, 0.4% Ho, and a dimension of 5 mm×5 mm in cross section and 2.5 mm in length. A plane-concave resonator is employed to make the system very simple and compact. The near hemispherical resonant is formed between the planar crystal front face and the output coupler. A dichromatic coating on the front face of the crystal is high transmitting at 792 nm but is totally reflecting at 2 μm. The other face is only polished and uncoated at both pump and output wavelengths. To efficiently remove the heat generated with pump power from the crystal, the crystal is wrapped with indium foils and held in brass heat sink. Temperature of the heat sink is held at a constant 283 K with a thermoelectric cooler. The laser cavity length is about 45 mm. The radius of curvature of the output coupler is near 52 mm and its transmittance to 2 μm laser is 2%. For passive Q-switch operation, a Cr:ZnS saturable absorber with a dimension of 9.3 mm×4.5 mm in cross section and 2.2 mm in length is inserted between the output coupler and the Tm,Ho:YLF crystal, and the distance of the Cr:ZnS crystal from the Tm,Ho:YLF crystal is L. The faces of Cr:ZnS crystal are antireflection coated near 2055 nm leading to an initial transmission of $T_0=95\%$. The laser pulse width, repetition frequency, and waveform are observed with a room temperature InGaAs detector and a TDS3032B digital oscilloscope. An energy meter (Coherent PS10) is employed to measure the pulse energy.

3. Results and discussion

When the distances L is 5 mm and 30 mm respectively, the average output power and pulse energy as a function of pump power are shown in Fig. 2. From Fig. 2(a), it can be noted that for L=5 mm the average output power increases from 6 mW to 16 mW with the pump power when the pump power is less than 1.7 W, then decreases with the pump power due to the thermal effect of Tm,Ho:YLF laser crystal when the pump power is over 1.7 W. For L=30 mm, the maximum average output power is 8 mW when the pump power is 1.5 W, then the average output power decreases with the pump power. Fig. 2(b) shows that the pulse energy at L=30 mm slightly increases from 5 μJ with the pump power, and arrives a maximum value of 6 μJ at the pump power of 1.5 W. It can also be noted from Fig. 2 (b) that the pulse energy increases slightly with the pump power for L=5 mm, but nearly a constant of 4 μJ. Fig. 3(a) shows the pulse width as a function of pump power. It can be seen that the pulse width at L=30 mm decreases from 3.7 μs to 2 μs as the pump power increases from 1 W to 1.7 W, however, the pulse width at L=5 mm exhibits no obvious dependence on the pump power and almost a constant of 1.25 μs. Fig. 3(b) gives the dependence of pulse repetition frequency on the pump power. It is seen from Fig. 3(b) that at L=5 mm the pulse repetition frequency linearly increases with the pump power from 1.3 kHz to 2.6 kHz when the pump power is increased from 1 W to 1.4 W, however, the pulse repetition frequency decreases with the pump power from 2.6 kHz to 1.8 kHz when the pump power is increased from 1.4 W to 1.9 W. The pulse repetition frequency at L=30 mm is at the range of 0.6–1.4 kHz when the pump power is changed between 1 W and 1.7 W. Through above experimental results, it can be

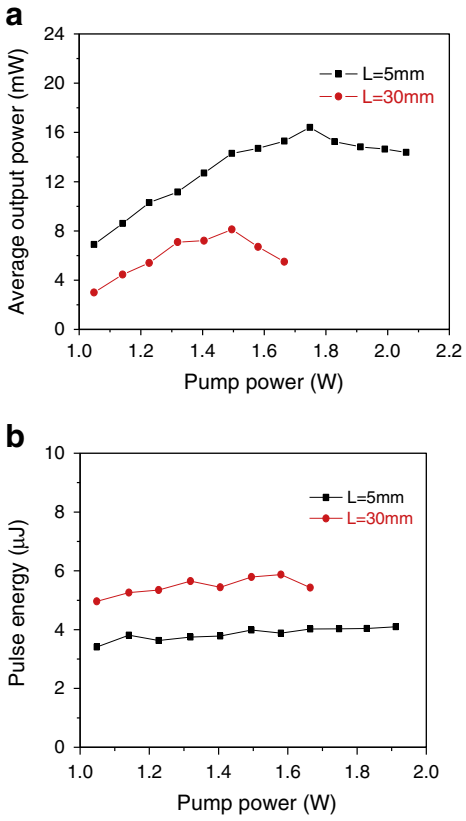

Fig. 2. (a) Average output power and (b) pulse energy as a function of pump power, and L is the distance of the Cr:ZnS crystal from the Tm,Ho:YLF crystal.

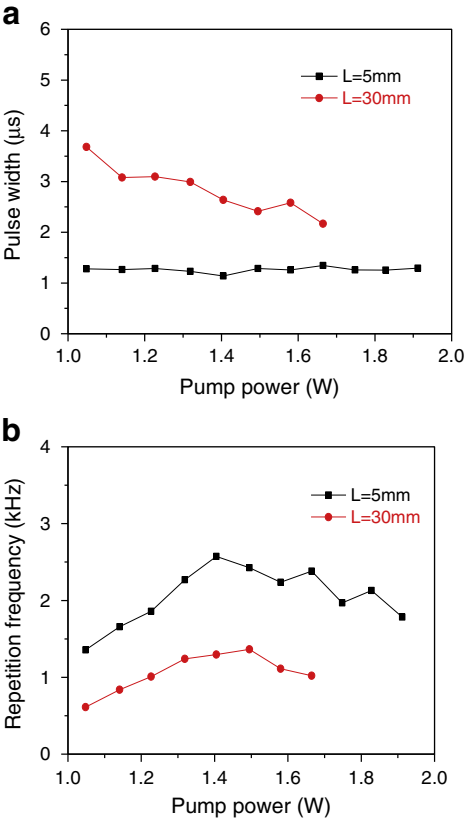

Fig. 3. (a) Pulse width and (b) repetition frequency as a function of pump power, and L is the distance of the Cr:ZnS crystal from the Tm,Ho:YLF crystal.

noted that when the distance L is about 5 mm, the passively Q-switched Tm,Ho:YLF laser shows special performance. The pulse energy and pulse width are nearly constants when the pump power is changed from 1 W to 1.9 W, however, the pulse repetition frequency can be tuned from 1.3 kHz to 2.6 kHz by only changing the pump power.

Q-switched Tm,Ho:YLF lasers have significant thermal lens effect which affects the stability of the laser resonator. To understand the experimental results better, we give the following theoretical analysis. An energy level diagram for Tm,Ho:YLF laser is shown in Fig. 4. When the 792 nm pump light from the diode laser is absorbed into the $^3H_4$ manifold, the $^3F_4$ manifold is efficiently populated through the well-known two-for-one cross-relaxation process. A fraction of the energy stored in the Tm^{3+} $^3F_4$ manifold is then transferred to the Ho^{3+} $^5I_7$ manifold. As the populations of $^3F_4$ and $^5I_7$ grow, the long lifetimes of the levels are reduced by energy transfer upconversion (ETU) processes, among which the most effective is $^3F_4+{}^5I_7\rightarrow{}^3H_6+{}^5I_5$. The excitation is followed by a fast decay to $^5I_6$, a transfer of excitation to $^3H_5$, and a fast relaxation to $^3F_4$. The heat generated from ETU processes is due to the multi-phonon relaxation from the excited level back to the upper laser level. The laser emission at 2.06 μm is due to a transition between the lowest Stark level in the $^5I_7$ manifold and a high level in the $^5I_8$ ground-state manifold. In such cases, the population density on the lower laser level is not presumed to be zero, but is assumed to have a small thermal population. The energy transfer between the Tm^{3+} $^3H_4$ and Ho^{3+} $^5I_7$ manifolds is fast compared to their upper state lifetimes, so they can be treated as a coupled level under CW pumping [23]. Under taking ETU effects into account, the rate equation for population density before laser oscillating is given by [23]

$$N_2 = N_{Tm} - N_1 \tag{1}$$

$$N_5 = N_{Ho} - N_4 \tag{2}$$

$$N_2 + N_5 = (1-f_{Ho})N_u + f_{Ho}N_u = N_u \tag{3}$$

$$\frac{dN_u}{dt} = R_p - \frac{N_u}{\tau} - QN_u^2 \tag{4}$$

where N_1, N_2, N_4 and N_5 are $^3H_6$, $^3F_4$, $^5I_8$ and $^5I_7$ population densities respectively, N_u is the sum of the Tm^{3+} $^3H_4$ and Ho^{3+} $^5I_7$ population densities, Q is the ETU constant, f_{Ho} is the net transfer energy from Tm^{3+} to Ho^{3+}, and τ is the coupled upper level lifetime and can be expressed as

$$\frac{1}{\tau} = \frac{1-f_{Ho}}{\tau_2} + \frac{f_{Ho}}{\tau_5} \tag{5}$$

where τ_2 and τ_5 are the intrinsic radiation lifetimes of the Tm^{3+} $^3F_4$ and Ho^{3+} $^5I_7$ levels. R_p is the average pump intensity and can be expressed as

$$R_p = \frac{\eta_p \eta_\alpha P_{in}}{h\nu_p} \frac{1}{\pi\omega_p^2 l} \tag{6}$$

where $h\nu_p$ is the pump photo energy, P_{in} is the incident pump power, η_p is the pump quantum efficiency and is primarily concentration dependent, ω_p is the average pump size in the crystal length, $\eta_\alpha = 1-\exp(-\alpha l)$ is the absorption efficiency at the pump wavelength, α is the absorption coefficient. From Eq. (4), the initial population density of the coupled upper level at the end of the high- loss segment at repetition frequency f can be derived as [24,25]

$$N_i = \frac{1}{B}\left[A\frac{\left(1+BN_f+A\right)+\left(1+BN_f-A\right)\exp(-A/\tau.f)}{\left(1+BN_f+A\right)-\left(1+BN_f-A\right)\exp(-A/\tau.f)} - 1\right] \tag{7}$$

$$A = \sqrt{1+4\tau^2 Q R_p} \tag{8}$$

$$B = 2Q\tau \tag{9}$$

$$N_f = \frac{\Delta n_f + f_l N_{Ho}}{\gamma f_{Ho}} \tag{10}$$

$$\Delta n_f = \frac{\delta}{2\sigma_e l} \tag{11}$$

$$\gamma = f_u + f_l \tag{12}$$

where N_f is the residual population inversion density of the coupled upper laser level from the preceding pulse, Δn_f is the residual population inversion density of the upper laser level from the preceding pulse, σ_e is the stimulated emission cross section, l is the crystal length, and δ is the roundtrip dissipated optical loss. γ is the inversion reduction factor, f_l is the fraction of the lower manifold.

Without ETU effects, i.e. Q = 0, from Eq. (4), the initial population inversion density of the coupled upper level at the end of the high-loss segment at repetition frequency f can be simplified as

$$N_i^0 = R_p\tau - \left(R_p\tau - N_f\right)\exp\left(-\frac{1}{\tau.f}\right) \tag{13}$$

With Eqs. (7) and (13), the fractional reduction of the coupled upper level population inversion density that is due to ETU effects can be expressed as [24]

$$F_{ETU}(f, P_{in}) = 1 - \frac{N_i}{N_i^0} \tag{14}$$

The parameter F_{ETU} is a function of the pump power and the repetition frequency. Since F_{ETU} represents the fraction of the ions in the coupled upper level via ETU process, the fraction $(1-F_{ETU})$ of the coupling upper level populations that decay via the fluorescence process results in the thermal loading equal to the quantum defect.

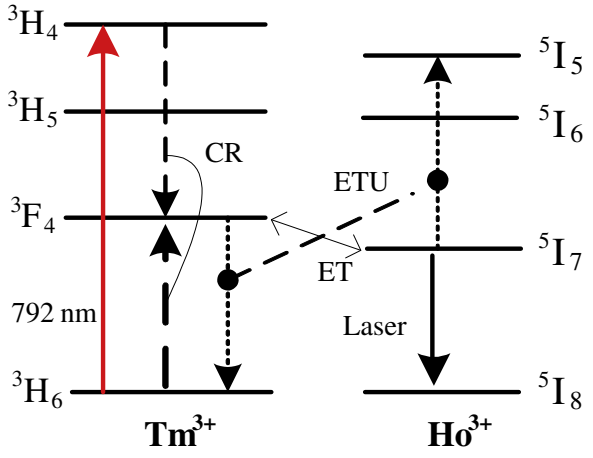

Fig. 4. Schematic diagram of the major excitation and relaxation processes in Tm,Ho: YLF laser crystal: CR, cross-relaxation; ET, energy transfer; ETU, energy transfer upconversion.

Under considering the relaxation efficiency, the fractional thermal loading can be expressed as

$$\xi(f,P_{in}) = \left(1-\frac{\eta_p}{2}\right) + \left\{F_{ETU}(f,P_{in}) + [1-F_{ETU}(f,P_{in})]\left(1-\frac{2\lambda_p}{\lambda_f}\right)\right\}\frac{\eta_p}{2} \tag{15}$$

where λ_p is the pump wavelength, $\lambda_f \approx 2$ μm is the average fluorescence wavelength. With Eqs. (7)–(15) and the following parameters: $\eta_p = 1.57$ [26], $\alpha = 5.4\ cm^{-1}$ [4], $\tau = 10$ ms [4], $\sigma_e = 15\times10^{-20}\ cm^2$ [27], $N_{Ho} = 5.59\times10^{19}\ cm^{-3}$, $l = 2.5$ mm, $\lambda_p = 792$ nm, $\lambda_l = 2.06$ μm, $\omega_p = 130$ μm, $Q = 5\times10^{-18}\ cm^3/s$, $\delta = 0.03$, we calculate the fractional thermal loading as a function of the repetition frequency for several values of the pump power as shown in Fig. 5(a). It can be noted that the fractional thermal load is more significant at low repetition frequencies because of the ETU effects. The thermal focal length for an end-pumped solid state laser is given by [9]

$$f_{th} = \frac{\pi K_c \omega_p^2}{\xi \eta_\alpha P_{in}} \frac{1}{[\partial n/\partial T + n(1+\nu)\alpha_T]} \tag{16}$$

where K_c is the thermal conductivity, $\eta_\alpha = 1\text{-}\exp(-\alpha l)$ is the absorption coefficiency, where α is the absorption coefficient, and l is the length of the laser crystal, ω_p is the average pump size in the active medium, ν is Poisson's ratio, α_T is the thermal expansion coefficient, n is the refractivity index of the laser crystal, $\partial n/\partial T$ is the thermal-optic coefficient of n. Taking the thermal lens effect into account, the mode size of laser can be given by

$$\omega_0 = \left[\left(\frac{\lambda}{\pi}\right)^2 \frac{L_e(2f_{th}-L_e)(R_2-L_e)(2f_{th}+R_2-L_e)}{(2f_{th}+R_2-2L_e)^2}\right]^{\frac{1}{4}} \tag{17}$$

where L_e is the optical cavity length, and R_2 is the radius of curvature of the output coupler. With Eqs. (16) and (17), Fig. 5(a), and the following parameters [28]: $K_c = 6\ W\ K^{-1}\ m^{-1}$, $n = 1.47$, $\alpha_T = 13\times10^{-6}\ K^{-1}$, $\partial n/\partial T = -4.3\times10^{-6}\ K^{-1}$, $\nu = 0.33$, $\alpha = 5.4\ cm^{-1}$, $\omega_p = 130$ μm, $L_e = 4.5$ cm, $R_2 = 52$ mm, the dependence of the mode size of laser on the pump power is calculated, and the calculation results for several repetition frequencies are shown in Fig. 5(b). It is clear from Fig. 5(b) that the influence of the thermal lens effect to the laser mode size is decreasing function of repetition frequency. The lower the repetition frequency, the larger the thermally induced loss, consequently, the faster the laser resonator becomes unstable as the pump power increases.

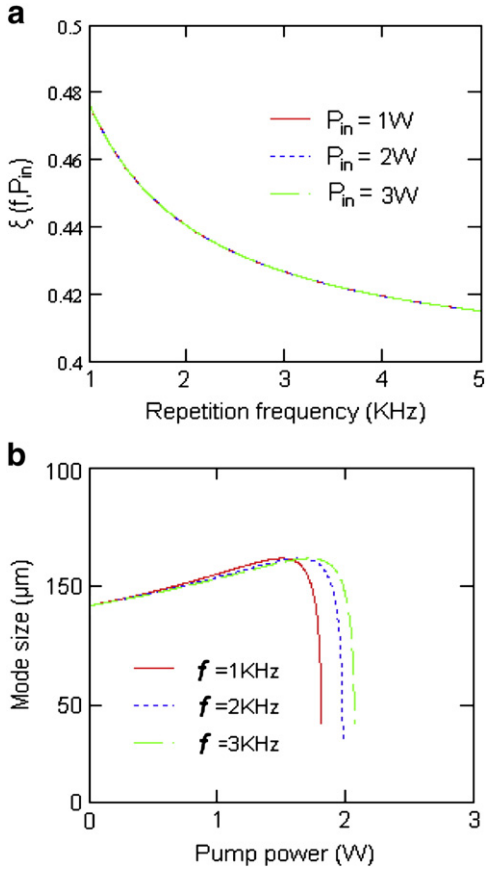

Fig. 5. (**a**) Dependence of ξ on the pulse repetition frequency for several pump powers.(**b**) Dependence of the mode size on the pump power for several pulse repetition frequencies.

According to the above theoretical analysis, the passively Q-switched Tm,Ho:YLF laser has prominent thermal effects, so the output power of the laser begins to decrease when the pump power is over a certain value as shown in Fig. 2(a). Because the pulse repetition frequency is higher at L = 5 mm than at L = 30 mm, the corresponding pump power that the average output power begins to fall is smaller at L = 30 mm than at L = 5 mm. The saturation absorption loss of Cr:ZnS saturable absorber is larger at L = 30 mm than at L = 5 mm due to the distribution of intracavity laser field, so the output power is higher at L = 5 mm than at L = 30 mm.

When the pump power is 1.4 W, the typical output pulse trains and individual pulses at L = 30 mm and L = 5 mm obtained from the Tm,Ho:YLF lasers are shown in Fig. 6. It can be noted from Fig. 6(a) that when the distance L is equal to 30 mm, the pulse amplitude variation of pulse-to-pulse stability is less than 10%, and the pulse repetition frequency is about 1.3 kHz. Fig. 6(b) shows that for a pump power of 1.4 W, the width of the single laser pulse in is about 2.7 μs. When the distance L is 5 mm, the pulse amplitude is more stable, and the pulse repetition frequency has a larger value of 2.6 kHz as shown in Fig. 6(c). Fig. 6(d) shows the pulse width is about 1.25 μs at L = 5 mm for a pump power of 1.4 W. Furthermore, the output pulses always show good stability, when the pump power is changed.

The emission wavelengths of the continuous wave free running and passively Q-switched Tm,Ho:YLF lasers are measured with a WDG-30 monochrometer which is connected to a cooled InGaAs photodetector. When the Tm,Ho:YLF laser is CW operation and the Cr:ZnS crystal is not placed in the cavity, the centre wavelength of the output laser is 2067 nm. However, when Cr:ZnS crystal is placed into the cavity, and the Tm,Ho:YLF laser is passively Q-switched operation, the centre wavelength of the output laser pulse is changed to 2053 nm as shown in Fig. 7.

When the distance L from the Tm,Ho:YLF crystal to the Cr:ZnS is 5 mm, the transverse output beam profiles are measured with a beam analyzer (Electrophysics, MicronViewer 7290A), and shown in Fig. 7(a) and (b). The output beam is close to fundamental transverse electromagnetic mode (TEM_{00}). The M^2 factors for various pump powers were measured by the traveling knife-edge method, and it can be noted that M^2 factors are less than 1.4 for various pump powers. So the TEM_{00} output beam is achieved in such compact passively Q-switched Tm,Ho:YLF laser with Cr:ZnS as a saturable absorber.

4. Conclusion

Laser diode end-pumped passively Q-switched Tm,Ho:YLF lasers near room temperature have been reported. The Q-switching operation is obtained by inserting a 2.2 mm thick Cr:ZnS crystal into the laser cavity. Compared to the output wavelength of 2067 nm in CW operation, the output wavelength of the passively Q-switched Tm,

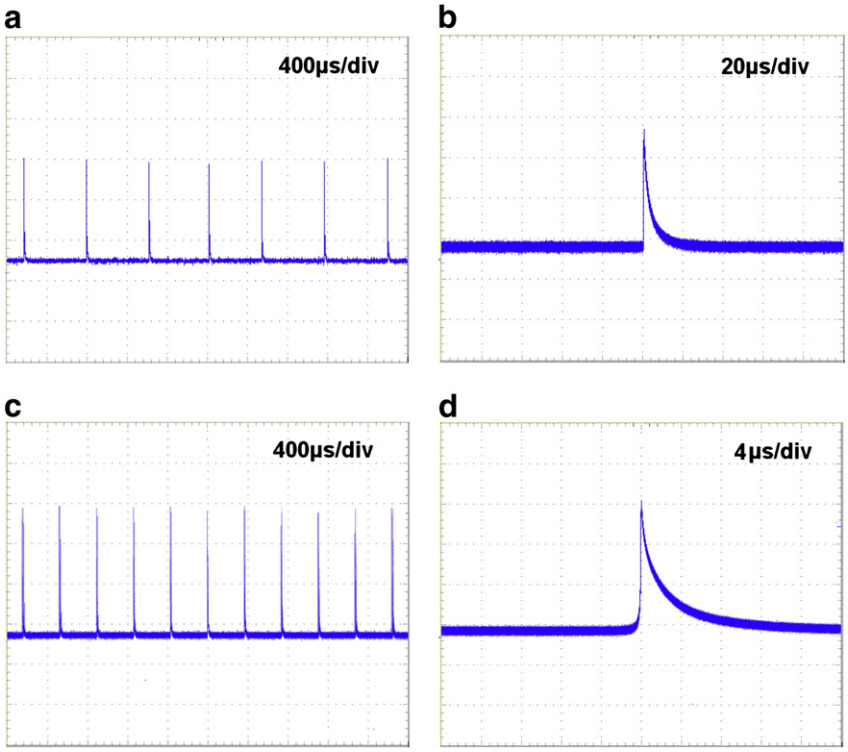

Fig. 6. (a) The train of output pulses at a repetition frequency of 1.3 kHz and (b) the expanded shape of the output single pulse showing 2.7 μs pulse width (L = 30 mm). (c) The train of output pulses at a repetition frequency of 2.6 kHz and (d) temporal profile of the output single pulse showing 1.25 μs pulse width (L = 5 mm).

Ho:YLF laser is 2053 nm. When the distances between the Cr:ZnS crystal and the Tm,Ho:YLF crystal are 5 mm and 30 mm respectively, the experimental results are compared. For the distance of 30 mm between the Cr:ZnS crystal and the Tm,Ho:YLF crystal, the maximal values of the output power and pulse energy are 8 mW and 6 μJ respectively, and the pulse width decreases with the pump power. For the distance of 5 mm, the laser beam profile is close to TEM_{00} mode, furthermore, the pulse width and the pulse energy are almost constants. The pulse width is about 1.25 μs, and the pulse energy is about 4 μJ. The nearly diffraction-limited and stable long pulse laser can be used to 2 μm laser lidar systems for accurate wind velocity measurements.

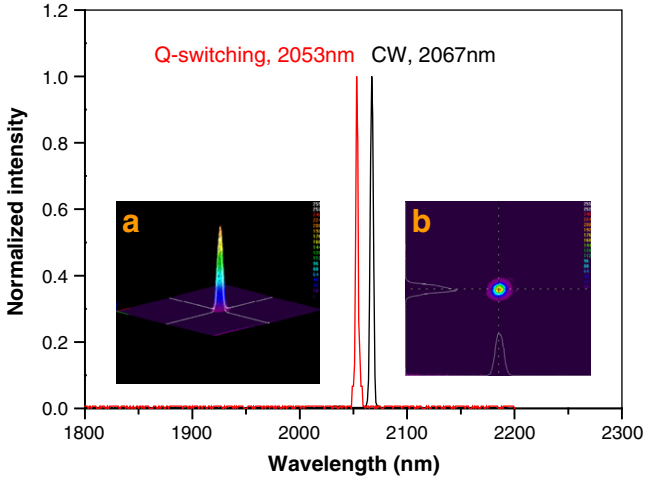

Fig. 7. Output laser spectra of the continuous wave free running and passively Q-switched Tm,Ho:YLY lasers. The insets show transverse beam profiles, (a) 3-dimension profile, and (b) 2-dimension profile.

Acknowledgements

The authors acknowledge financial support of the Specialized Research Fund for the programe for New Century Excellent Talents in University (Grant No. 2011269), the National Natural Science Foundation of China (Grant Nos.10804022 and 60878016), Natural Science foundation of Heilongjiang Province (Grant No. A200801) and the Innovation Talents Foundation of Harbin City (Grant Nos. 2008RFQXG026 and 2009RFQXG054), and the Fundamental Research Funds for the Central Universities (Grant Nos. HEUCFZ1021 and HEUCF20101109).

References

[1] J. Yu, B.C. Trieu, E.A. Modlin, Optics Letters 31 (4) (2006) 462.
[2] O.A. Louchev, Y. Urata, S. Wada, Optics Express 15 (7) (2007) 3940.
[3] B.M. Walsh, N.P. Barnes, M. Petros, J. Yu, U.N. Singh, Journal of Applied Physics 95 (7) (2004) 2772.
[4] G.L. Bourdet, G. Lescroart, Applied Optics 38 (15) (1999) 3275.
[5] K. Yang, H. Bromberger, H. Ruf, H. Schäfer, J. Neuhaus, T. Dekorsy, C.V. Grimm, M. Helm, K. Biermann, H. Künzel, Optics Express 18 (7) (2010) 6537.
[6] A.A. Lagatsky, F. Fusari, S. Calvez, S.V. Kurilchik, V.E. Kisel, N.V. Kuleshov, M.D. Dawson, C.T.A. Brown, W. Sibbett, Optics Letters 35 (2) (2010) 172.
[7] G. Galzerano, E. Sani, A. Toncelli, G.D. Valle, S. Taccheo, M. Tonelli, P. Laporta, Optics Letters 29 (7) (2004) 715.
[8] C. Nagasawa, D. Sakaizawa, H. Hara, K. Mizutani, Optics Communications 234 (1–6) (2004) 301.
[9] X. Zhang, Y. Ju, L. Li, Y. Wang, Journal of Physics D: Applied Physics 40 (22) (2007) 6930.
[10] I.F. Elder, M.J.P. Payne, Electronics Letters 34 (3) (1998) 284.
[11] X. Zhang, Y. Ju, Y. Wang, Optics Express 13 (11) (2005) 4056.
[12] X. Zhang, Y. Wang, Optics Letters 32 (16) (2007) 2333.
[13] Y.K. Kuo, M. Birnbaum, W. Chen, Applied Physics Letters 65 (24) (1994) 3060.
[14] Y.K. Kuo, M. Birnbaum, Applied Optics 35 (6) (1996) 881.
[15] Y.K. Kuo, M. Birnbaum, F. Unlu, M.F. Huang, Applied Optics 35 (15) (1996) 2576.
[16] T. Tsai, M. Birnbaum, Applied Optics 40 (36) (2001) 6633.
[17] L.E. Batay, A.N. Kuzmin, A.S. Grabtchikov, V.A. Lisinetskii, V.A. Orlovich, A.A. Demidovich, A.N. Titov, V.V. Badikov, S.G. Sheina, V.L. Panyutin, M. Mond, S. Kück, Applied Physics Letters 81 (16) (2002) 2926.
[18] B. Yao, Y. Tian, G. Li, Y. Wang, Optics Express 18 (13) (2010) 13574.
[19] F.Z. Qamar, T.A. King, Optics Communications 248 (4–6) (2005) 501.
[20] S.D. Jackson, Applied Optics 46 (16) (2007) 3311.
[21] M.G. Jani, F.L. Naranjo, N.P. Barnes, K.E. Murray, G.E. Lockard, Optics Letters 20 (8) (1995) 872.

[22] P.J.M. Suni, S.W. Henderson, Optics Letters 16 (11) (1991) 817.
[23] X. Zhang, Y. Wang, L. Li, Y. Ju, Y. Peng, Journal of Physics D: Applied Physics 42 (2) (2009) 025107.
[24] Y.F. Chen, Y.P. Lan, S.C. Wang, Journal of the Optical Society of America B: Optical Physics 19 (7) (2002) 1558.
[25] Y.P. Lan, Y.F. Chen, S.C. Wang, Applied Physics B 71 (1) (2000) 27.
[26] B.T. Mcguckin, R.T. Menzies, H. Hemmati, Applied Physics Letters 59 (23) (1991) 2926.
[27] M.E. Storm, IEEE Journal of Quantum Electronics 29 (2) (1993) 440.
[28] J. Harrison, R.J. Martinsen, IEEE Journal of Quantum Electronics 30 (11) (1994) 2628.